This is a peer-reviewed, accepted author manuscript of the following research article: Rizzuto, F, Corney, J, Dempster, W & Tijsseling, A 2024, 'An improved positive displacement pump model accounting for suction cavitation', Journal of Pressure Vessel Technology, vol. 146, no. 4, 041404. https://doi.org/10.1115/1.4065564

An improved positive displacement pump model accounting for suction cavitation

Francesco Rizzuto, PhD, Department of Mechanical and Aerospace Engineering, University of Strathclyde, Glasgow, United Kingdom, Francesco.rizzuto.fr@gmail.com

Jonatan Corney, Department of Digital Design and Manufacture, University of Edinburgh, Edinburgh, United Kingdom

William Dempster, Department of Mechanical and Aerospace Engineering, University of Strathclyde, Glasgow, United Kingdom

Arris Tijsseling, Department of Mathematics and Computer Science, Eindhoven university of technology, Eindhoven, Netherlands

Abstract

Positive displacement (PD) pumps are widely employed in industrial settings due to their inherent simplicity and reliability, serving a variety of applications from slurry transport to jet washing. Although their operational principles are straightforward, the fluid dynamics of the pumped medium exhibit non-trivial characteristics, including intricate transient phenomena. Consequently, a comprehensive fluid dynamic description, such as a three-dimensional fluid analysis, presents challenges due to its demanding computational requirements. While simpler analytical PD pump models are available, they often fail to adequately represent the primary system behaviours, particularly when dealing with cavitation. Motivated by these challenges, this study aims to develop a novel one-dimensional model for PD pumps, offering a representation of essential fluid phenomena without imposing significant computational burdens. After assessing the relative importance of the fluid dynamic behaviours that the model must capture, we construct a pump model based on a one-dimensional fluid description and solve it using a second-order in time and space MUSCL-TVD scheme. The model's validity is confirmed by its application to both single-chamber and three-chamber diaphragm PD pumps, which are instrumented for experimental validation. The results of the one-dimensional model exhibit strong agreement with physical experiments, both in controlled laboratory environments and field conditions. This success suggests a promising approach for industrial applications.

Nomenclature

Acronyms

BDC	Bottom dead centre
CFD	Computational Fluid Dynamics
CFL	Courant Friedrichs Lewy Condition
DGCM	Discrete Gas Cavity Model
MUSCL	Monotone Upwind Scheme for Conservative Law
ODE	Ordinary differential equation
PD	Positive Displacement Pump
PDE	Partial differential equation
RANS	Raynolds Averaged Navier Stokes
TVD	Total variation diminishing

Variables

α	volume fraction
ρ	Density [kg/m^3]
Θ	Multistep coefficient
Ω	Multi-stage coefficient
ε	Relative roughness
ζ_i	loss of the valve
Δ	difference
λ	eigenvalue
Λ	pump piston design parameter
ω	angular velocity [rad/s]

ψ	Pressure force coefficient
A	Area of the valve [m^2]
c	speed of sound [m/s]
D_h	Hydraulic diameter [m]
F_D	Damping force [N]
F_m	Gravity force [N]
F_{pre}	Preload spring force [N]
F_p	Pressure force [N]
F_s	Spring force [N]
f	Darcy friction factor velocity
l_{gap}	gap length of the valve [m]
p	Pressure [Pa]
P	polynomial characteristic function
r	radius [m]
R_{xy}	correlation factor
Re	Reynolds number
S_x	Source term in the momentum equation
t	time [sec]
U	State variable
u	Fluid velocity [m/s]
x	axial coordinate [m]
$\dot{x}$	velocity [m/s]
$\ddot{x}$	acceleration [m/s^2]

V	Volume [m^3]
k	polytropic index

Subscription

$down$	downwards
exp	experiment
i	index
L	liquid
num	numerical
m	mixture
p	piston
up	upwards

Introduction

Basics principles of positive displacement pump

Positive displacement pumps (PD) are simple and reliable machines capable of generating high pressures mostly independently from the applied load. Their straightforward mechanical configuration involves a reciprocating displacement motion, engendering compression within a confined volume to supply the requisite pressure. Widely employed in robust sectors such as mineral extraction, power generation, and oil & gas exploration. They exhibit diverse designs, incorporating liquid displacement mechanisms like pistons, plungers, or diaphragms. Distinct designs exhibit specific operational characteristics; for example, the inclusion of a diaphragm plays a pivotal role in augmenting the pump's reliability. This is achieved by isolating the working fluid from the mechanical components, contributing to enhanced operational robustness. To explain the main functionality of the pump component, a typical diaphragm pump cross-section is presented in Figure 1. It is noteworthy that the delineation provided herein can be extended to piston and plunger pumps owing to their more straightforward design. In detail, referring to Figure 1, the crankshaft (1) is driven by an external engine, typically an electrical or internal combustion engine. This linkage is established through a gearbox, facilitating the transmission of motion and power to the pump mechanism. The kinetic energy is transmitted to the piston (6) via an interconnected arrangement of connecting rods and couplings (3-6). In the context of mechanically driven diaphragm pumps, the diaphragm (9) is directly attached to the piston rod (5), establishing a direct mechanical linkage. For a hydraulically driven pump, a propellant liquid (15) intervenes between the piston and the diaphragm. This intermediary fluid serves the purpose of mitigating mechanical stresses imposed on the diaphragm during operation. Under this arrangement, the diaphragm acts as a barrier, effectively segregating the working fluid (16) from the driving section. Two valves (11-12) are mounted at each end of the pumping chamber (14) to determine the compressing volume. Suction and discharge ducts (16,19) are normally included in the design. For both discharge (17) and suction (18) lines, a hydraulic accumulator (10) or air vessel (13) can be used to dampen the pressure fluctuations in the system.

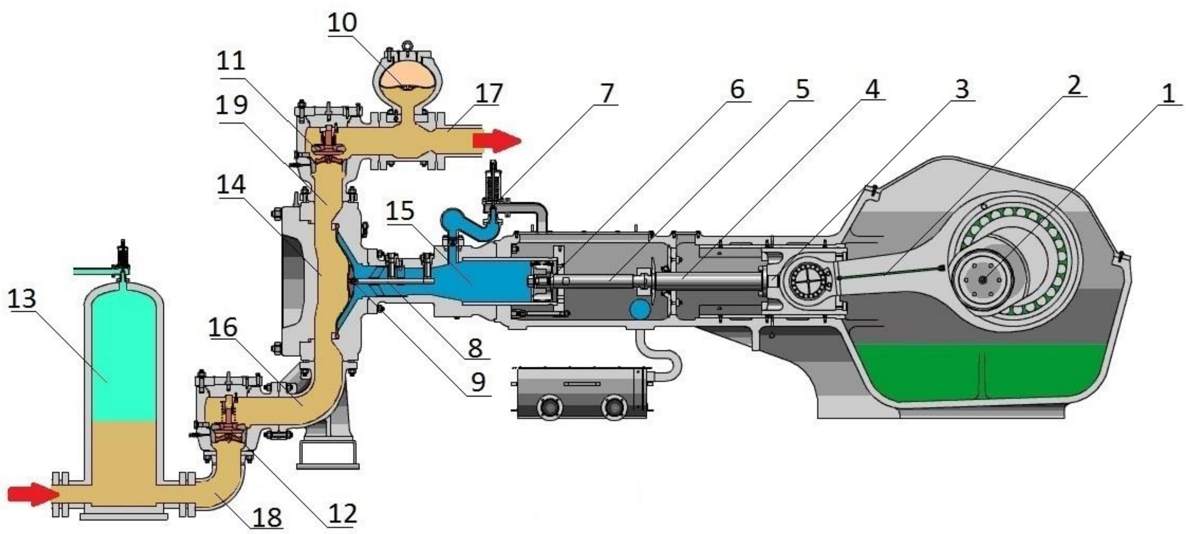

Figure 1 - Cross-section of GEHO® piston pump.

This mechanism generates a theoretical pressure cycle that recurs every 360 degrees. However, due to different frequency responses of the hydraulic component, slight variations in the cycles can occur. To simplify the description of the pump cycle, the piston is conceptualized in its retracted position, denoted as the bottom dead centre (BDC), situated at the zero-crank position. The compression phase initiates with an outward displacement of the piston or diaphragm, theoretically commencing immediately as the suction valve (12) is closed. Nevertheless, the inertia of the valve and the intricacies of fluid dynamics may introduce delays, leading to a lag in the compression phase. During this stage, there is a potential for the discharge phase to overlap with the closure of the suction valve, giving rise to operational losses. Once the suction valve is closed, the pressure within the piston chamber (15) rapidly ascends until it attains the opening pressure of the discharge valve. This pressure reaches a slightly higher value than the discharge plenum pressure partly due to the valve acting forces (inertia, spring, and pre-load force and pressure forces). Similarly, for the discharge valve closure and opening, the suction valve delays will occur introducing a decrease in pumping performance.

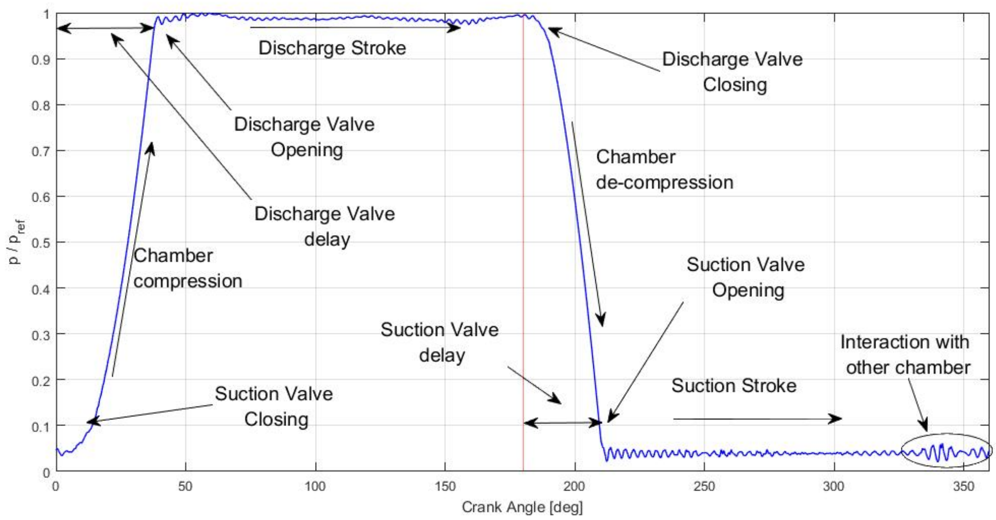

Figure 2 – Example of pressure cycle for a PD pump with measurements taken from the chamber.

To provide clarity, a normalized pressure response for a single chamber cycle is illustrated in Figure 2. This graphical representation was generated using a pressure transducer directly interfaced with the pump chamber, offering a comprehensive depiction of the pressure variations throughout the operational cycle. Table 1 presents the typical range of valve opening and closing movements in terms of crankshaft angle. This information provides a quantitative reference for the angular displacement associated with the initiation and termination points of valve actions within the pump mechanism.

Table 1 - Opening and close Valve delay [1]

	Opening Delay [deg]	**Closing Delay [deg]**
Suction Valve	20 – 45	5 - 10
Discharge Valve	20 – 45	5 – 10

The complexity of the cycle is further extended by the possible formation of cavitation, expansion of non-dissolved gas, and the interaction of pressure waves with other components or chambers for multi-chamber pumps. The inception of cavitation is notably prevalent during the suction phase, where low static pressures arise due to the acceleration of the fluid across the valve[2]–[8]. This second-phase phenomenon introduces further complexity to the operational dynamics of the pump system. If the vapor pressure at the local liquid temperature is reached, then cavitation can occur. Concurrently, non-dissolved gases may undergo expansion.

Considering the pure mechanical description, it becomes evident that the pump's performance is profoundly impacted by piston movement that in the first instance can be described by a sinusoidal formulation. Equation (1) represents the piston’s velocity profile with the design parameter $\Lambda = \frac{r}{l}$, where r is the crank radius and l is the connecting rod length.

$$\dot{x_p}(t) \approx r\omega \left[sin\, \omega t - \frac{\Lambda}{2} sin\, 2\omega t \right] \qquad (1)$$

When Λ is equal to zero the output manifests as a pure sinusoidal waveform. Nonetheless, this parameter holds paramount significance for pump efficiency. Λ exerts the potential aspect to mitigate issues such as cavitation. The careful consideration and adjustment of this parameter are essential in optimizing the overall performance and reliability of the pump system.

Literature review

As previously mentioned, the operational concept of the positive displacement (PD) pump may seem straightforward, relying on a reciprocating piston/diaphragm and self-acting valves. However, the intricacies arising from the interaction of these components make computational fluid dynamics analysis challenging. The dynamic interplay of forces, fluid flows, and valve actions necessitate a nuanced approach to comprehensively model and understand the pump's behaviour through computational simulations. The intricate flow interactions within the pump demand a thorough understanding and precise modelling of each component. Utilizing three-dimensional algorithms, especially those requiring a moving mesh for dynamic elements such as the piston and self-acting valves proves to be a challenging and computationally demanding task [2], [3], [7], [9]. Therefore, the full description of the fluid dynamics in a PD pump is expensive if not impractical for many industrial applications. The challenge is further increased in the case of multiple-cylinder pumps, commonly used in industry to increase flow rate and efficiency. The connection of the cylinders, due to a common suction and discharge chambers, results in a coupling between the chambers and hence affects the pump operating behaviour. In addition, initialization issues occur due to different phase shifts of the chambers. Consequently, few full CFD models are described in the literature, and they are mostly focused on a specific component; typically, the suction valves [2], [3], [9], [10] or diaphragm [11]. Differently complete networks [10], [12] consider a one-dimensional approach. Iannetti et al. [2], simulate only the suction phase where cavitation conditions occur and neglect the discharge phase and any interactions that the pump has with the overall hydraulic system. The same condition for a small diaphragm pump was performed by Li et al.[8] where organic fluid was considered. Therefore, no wave reflection and interaction with other chambers or the reservoir is considered. Iannetti et al.[2], [3] also highlight the importance of correctly tuning the value of the existence of non-condensable gas (NCG).

In contrast, the simplest models of reciprocating pumps are constructed from simply lumped parameter approaches [6], [13]–[16]. Shu et al. model [9] built upon Johnston's model [5], [6] developed a multi-chamber model with network interaction. Several simplifications were implemented: (1) the discharge flows of all the chambers are connected in one lumped point, (2) a small air pocket chamber is simulated in the suction line to consider a non-condensable gas, and (3) volume parameters are introduced to calculate the effective bulk modulus of the air-liquid flow. The latest condition implies tuning two different parameters to achieve accurate results. To compute the dynamics of the network, Shu et al. [14] used the Galerkin finite element method that considers frequency-dependent friction. Although their code predicted the behaviour of the pump network with acceptable accuracy, the algorithm was ineffective when cavitation occurred. Moreover, the authors highlighted the importance of the compressibility effect on the valve model to achieve good predictions. A different approach to analysing the dynamics of a system was given by Singh et al. [17]who for the first time studied a network of multiple PD pumps and their associated interaction. This was done in the frequency domain, normally used for steady pump conditions. They use an iterative process to calculate the pump behaviour and the pipe system response. At that time the method was a significant contribution to the field, although the complexity of the valves and the pump interaction was not well captured, being too simplistic for the complexity of the processes. The importance of valve modelling was highlighted by Johnston et al. [5], [6], who studied the valve dynamics and the cavitation conditions experimentally. Test data were used to determine a force coefficient and establish a semi-empirical simple valve model. The results considered the effects of different valve angles and the shape of the valve as major behaviour factors. Johnston's simulation [5], [6] agreed with the experiment in the non-cavitating regime. However, when cavitation occurred, even in small quantities, differences were found, emphasizing the significant impact that this phenomenon has on the pump performance.

Research involving purely cavitation in PD pumps was performed by Opitz et al. [4]. They categorized the cavitation phenomenon as *pseudo-cavitation, vapour cavitation, and gas cavitation*. The *vapour cavitation* condition is further refined into *incipient, partial, and full cavitation*. This categorization is important for a better understanding of the potentially harmful cavity condition. In addition, the authors' model calculates the amount of cavitation using a fluid velocity model that is related to the theoretical piston velocity. Although that model perfectly matches the cavitation produced in many cases, it does not give information on the pressure and flow, or the number of cavities produced and propagated in the system.

The propagation of information inside the hydraulic network in which a PD pump is embedded is vital to understanding the performance of the pump itself as pointed out by Vetter and Schweinfurter [18]. In their research, the generated pressure pulsations are related to the volumetric efficiency of the pump, for a different number of chambers. The main purpose was to simulate the pressure pulsation of an entire pump network using the ROLAST software, a one-dimensional code solving the continuity and momentum, using the method of characteristics. The predicted results agreed with different pump designs, although no cavitation algorithm was considered.

With the same logic, Josifovic et al. [12], used two different commercial codes to exploit the potential of one-dimensional approaches alongside three-dimensional RANS analysis. The three-dimensional model performed in Fluent environment determined the general hydraulic characteristics of the valve which were extrapolated into the one-dimensional model. Once more the limitation of the computational effort was highlighted, and good agreement was found with the experimental results when cavitation was not addressed. The use of two different software approaches limited the range of applicability. However, it has the benefit of establishing a better definition of the complex components, whereas in many other cases, commercial codes have the major drawback of modelling the dynamics of components with empirical coefficients. This results in the simplification of important phenomena, like valve backflow or energy losses in orifices.

Another major factor influencing the simulation accuracy of a positive displacement diaphragm pump is the interaction that the fluid has with the diaphragm. In the case of a hydraulically driven pump, the propelling liquid is interposed between the piston and the diaphragm due to structural reasons. Van Rijswick [1] studied the interaction that the diaphragm has with the surrounding fluid, using a three-dimensional fluid-structure interaction approach. In his research, the simplification of a mixture density description for both driven and slurry fluid was considered, a feasible approximation when the density of both fluids is comparable. This simplification opens the possibility of using a one-dimensional analysis of wave propagation not only for mechanical-driven pumps but also for fluid-driven pumps.

The simplest system of equations capable of describing the discussed complexity in one dimension is the water hammer equations. They are implemented with different algorithms and strategies, mainly using finite-difference approaches [19]–[24] or the finite volume method [25]–[30]. The main advantage of the finite volume methods is their ability to handle discontinuities in fluid behaviour. In addition to these algorithms, the use of a total variation diminishing (TVD) solver reduces the influence of numerical wiggle and noise [31]. Regarding the time integration strategy, water hammer equations are often solved explicitly, although the implicit schemes are more stable and time-efficient, they are limited by the distortion produced in wave propagation paths [32].

In conclusion, the complexity of the system, the importance of the second phase (air or/and vapour), the time-grid dependence, the cavitation model, and the simulation of the network are all important features highlighted in the literature. For this reason, this paper addresses those problems by discussing an overall improved model for the simulation of positive displacement pumps. The effect of pressure wave propagation, compressibility, non-condensable gas, and cavitation are accounted for and the simulation of multiple chambers and their interaction with pipeline networks is also implemented. The improved model is developed from a one-dimensional computational description making it computationally efficient and validated with experimental data for two different positive displacement diaphragm pump designs. The performance of the pump is numerically determined and compared with experimentally determined pressure values. In addition, pump efficiency frequency analysis, and indirect cavitation evaluation are given to better understand the pump conditions and performances.

Methodology

The diaphragm pump employed in this study is akin to the one depicted in Figure 1. The model used in this work closely resembles the physical configuration illustrated in the figure, providing a basis for the analysis and simulations conducted in the study.

To provide a comprehensive depiction of the pump, each constituent element, including the suction and discharge line ducts, chambers, and valves, is individually represented. This approach allows for a detailed analysis of the interactions among these components, facilitating a thorough understanding of the pump's operational dynamics. The modelling approach assumes axial flow, and for simplicity, three-dimensional phenomena are neglected. In the model, several mechanical components are represented by a lumped parameter approach including the suction, discharge valve and hydraulic accumulator.

Figure 3 shows the schematic and simplification of a positive displacement pump for a single chamber pump. The configuration consists of:

- *piston section*, (component 6, in Figure 1 and component 1, in Figure 3);
- *pre-chamber section* (component 15, in Figure 1 and component 2, in Figure 3);
- *chamber section* (component 14, in Figure 1 and component 3, in Figure 3), where the diaphragm dynamics are neglected [33], and the two fluids (propelling and working fluid) cannot physically interact but they can exchange momentum.
- *Suction and discharge section* (components 16 and 19, in Figure 1 and components 5 and 6, in Figure 3), representing the volume upstream of the valve;

- *Suction and discharge pipe* (components 17 and 18, in Figure 1 and components 6 and 7, in Figure 3), and the volume downstream of the suction valve and discharge valve (components 11 and 12, in Figure 1).

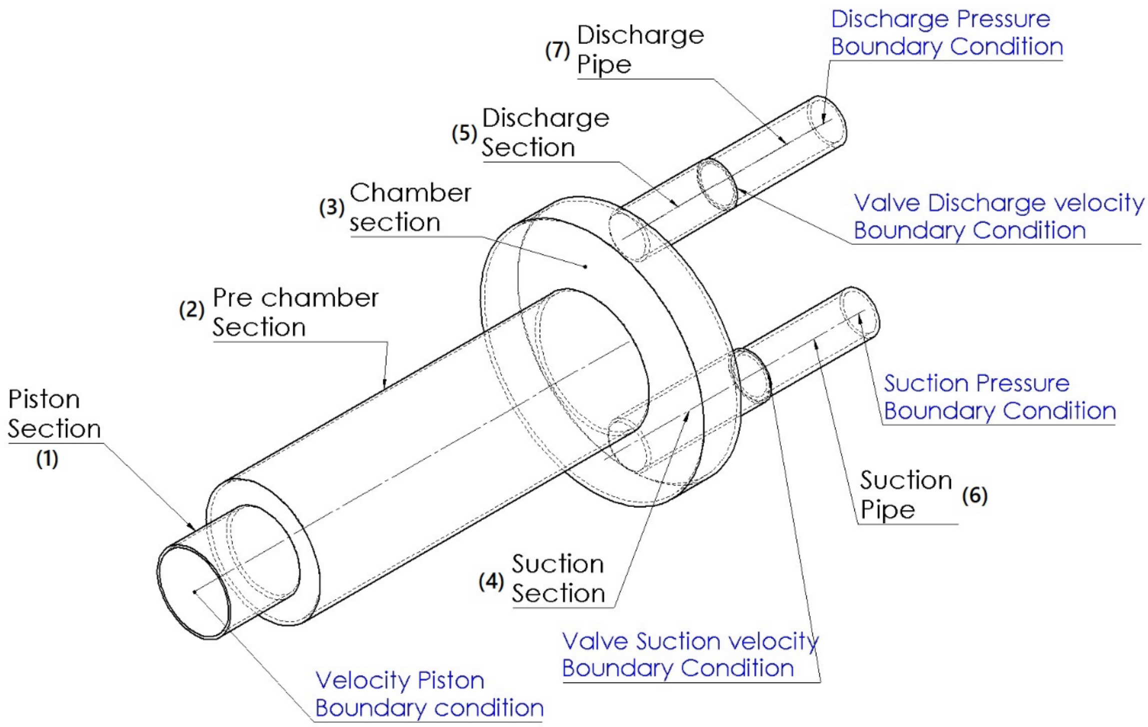

Figure 3 - Pump simplified schematic for one-dimensional analysis.

The intricate interplay between all pump components and the fluid itself forms a complex system. This complexity necessitates the computation of both the dynamic behaviours of the components and the fluid dynamics. A comprehensive understanding of these interactions is crucial for accurate modelling and simulation of the pump system.

Numerical Solution

The numerical simulation of the entire system demands simultaneous calculations for both fluid dynamics, described through a one-dimensional approach, and the dynamics of the mechanical components. The fluid dynamics model elucidates the fluid solution, while the mechanical component model provides insights into the mechanical dynamics. This dual-model approach ensures a holistic representation of the intricate interactions between the fluid and the mechanical elements within the pump system.

Fluid dynamics model

A comprehensive one-dimensional analysis of the pressure wave phenomenon in all fluid-based components is conducted through a complete one-dimensional fluid dynamic description. In this analysis, the temperature variation in the system is assumed to be negligible, rendering the system isothermal. Consequently, the energy equation is neglected, allowing the continuity and momentum equations, expressed as partial differential equations (PDEs), to accurately represent the hydraulics, as outlined in Equation (2):

$$\begin{cases} \frac{\partial \rho}{\partial t} + \frac{\partial \rho u}{\partial x} = 0 \\ \frac{\partial \rho u}{\partial t} + \frac{\partial (\rho u u + p)}{\partial x} = S_x \end{cases} \tag{2}$$

Where ρ is the density, u the fluid velocity, p the pressure and S_x the source term corresponds to the dissipation term.

The system is deemed hyperbolic when the Jacobian matrix of the system is diagonalizable with real eigenvalues. This system is weakly hyperbolic [34], [35] due to the eigenvalues being equal to $\lambda_1 = 0$ and $\lambda_2 = u$, thus, to solve this system a preconditioning matrix should be considered [35]. Implementing this methodology can be challenging, especially for complex systems involving multiple connections and diverse boundary conditions. To simplify the solution, the speed of sound c is introduced with the Newton–Laplace equation $c^2 = \frac{\partial p}{\partial \rho}$, decoupling the pressure and the density from the system of equations. The system then becomes strongly hyperbolic with two eigenvalues, reported in equation (3), that are always real, since $u^2 + 4c^2 > 0 \ \forall u, c$.

$$\begin{aligned} \lambda_1 &= \frac{u - \sqrt{u^2 + 4c^2}}{2} \\ \lambda_2 &= \frac{u + \sqrt{u^2 + 4c^2}}{2} \end{aligned} \tag{3}$$

Equation (2) is therefore simplified into equation (4)

$$\begin{cases} \frac{\partial p}{\partial t} + c^2 \frac{\partial \rho u}{\partial x} = 0 \\ \frac{\partial \rho u}{\partial t} + \frac{\partial (\rho u u + p)}{\partial x} = S_x \end{cases} \tag{4}$$

When neglecting the convective term in the momentum equation and applying the incompressible flow condition, the system reduces to a classical water hammer formulation.

To compute the dissipation term, the source term is evaluated with the step method [36]. In detail, the source term is equal to: $S_x = -\frac{1}{8}\phi\rho f\ u\,|u|$, where f is the Darcy friction factor and is determined using the Colebrook-White equation(5):

$$\frac{1}{\sqrt{f}} = -2\,log\left(\frac{\varepsilon}{3.7D_h} + \frac{2.51}{Re\sqrt{f}}\right) \tag{5}$$

Where the ratio $\frac{\varepsilon}{D_h}$ is the relative roughness and Re is the Reynolds number.

The numerical solution is progressed through an explicit finite volume method. The algorithms used a MUSCL scheme with a slope limiter to guarantee a TVD scheme, second order in time and space. This method has been previously implemented for the water hammer equation [29], showing good agreement with the experiment, even with the discrete cavity model. Differently from Zhou et al. [29], the code was developed to consider the change in the density and the speed of sound with the amount of volume fraction of generated vapour [37]. The description considers a homogeneous flow with two phases, liquid and gas, as a single fluid.

To reach the complete numerical solution, three different steps are performed.

- **Cell Boundary extrapolation:** a first-order reconstruction value is used considering the slope function given by the slope limiter $U_i^{R,L} = U_i \pm \frac{x-x_i}{\Delta x}\Delta U_i$, where $x\epsilon\left[x_{i-\frac{1}{2}}; x_{i+\frac{1}{2}}\right]$.
- **Evolution**: half-time step evaluation $\overline{U}_i^{R,L} = U_i^{R,L} - \frac{1}{2}\frac{\Delta t}{\Delta x}[f(U_i^R) - f(U_i^L)]$
- **Riemann solution:** solving the Riemann problem. $U_{i+\frac{1}{2}}(x) = \begin{cases} U_{i+1},\ x > x_{i+\frac{1}{2}} \\ U_i,\ x < x_{i+\frac{1}{2}} \end{cases}$

The solution without the source term is then performed for all pump sections independently. The source term is introduced using the fractional-step method [34]. This strategy allows the solution of the homogenous formulation of the system and the resulting system of the ordinary differential equation (ODE). To achieve good accuracy, a Runge-Kutta 4th order is used.

To address the cavity formation, a revisited Discrete Gas Cavity Model (DGCM) with compressibility already used by Rizzuto et al. [37] is considered. This method required an even mesh number to evaluate the lumped gas/vapour cavity. When the pressure of the fluid is calculated below the vapour pressure, the algorithm calculates the amount of the second phase formed across two boundaries and sets the pressure value at the two cells equal to the vapour pressure. At the same time, in the background, the pressure that the system should have computed is stored and compared with the vapour pressure value. The differences between the two pressure values (calculated and the vapour pressure) are used to evaluate the amount of vapour cavity formation and distribution across two cells, as shown in Figure 4.

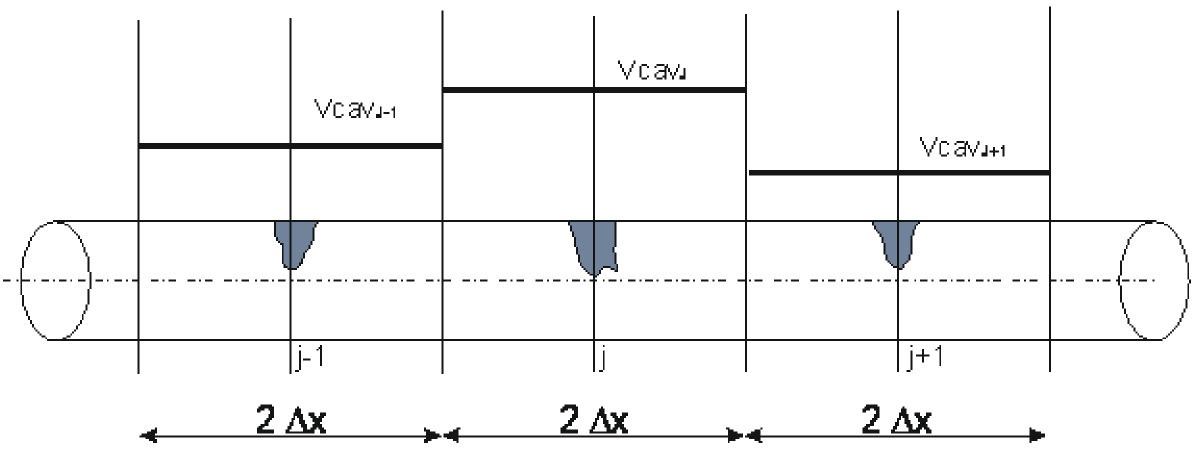

Figure 4 – Visual explanation of the cavitation grid formation

When all the cavity formation is performed, a piecewise linear function is used to evaluate the amount of the second phase formed across all the pipe sections.

At this point, both the density and the speed of sound of the mixture are calculated with the equation (6) used already by Rizzuto et al. [37] and described in detail by Brennen [38].

$$\begin{aligned} \rho_m &= \left[\rho_L\left(1-\textstyle\sum_i^N \alpha_i\right)+\textstyle\sum_i^N \alpha_i\,\rho_{\alpha_i}\right] \\ \frac{1}{c_m^2} &= \rho_m\left(\frac{\sum_i^N \alpha_i}{k\,p}+\frac{1-\sum_i^N \alpha_i}{\rho_L c_L^2}\right) \end{aligned} \quad (6)$$

Where p is the pressure; k the polytropic index, which is equal to 1 for an isothermal expansion; N the number of gas phases present in the mixture; and α_i is the volume fraction of the gas i. The speed of sound for pure water is calculated from the bulk modulus equation and the formulation given in [39]. However, the variation in the speed of sound due to the fluid-structure interaction is almost negligible due to the high stiffness of the thick pipe wall.

To summarize, the PDE is solved with the MUSCL scheme, while the ODE with the explicit formulation uses the Runge-Kutta method. This approach calculates the derivative of the function once in the initial and final time step and two times in the mid-step $\left(\frac{\Delta t}{2}\right)$. The combination of these four time points gives the unknown variable at the next time step allowing for the introduction of the dissipation terms in the system.

Mechanical component model

To provide a complete representation of a positive displacement pump, the auxiliary components which interact with the diaphragm also need to be accounted for. For this reason, modelling of the valves, hydraulic accumulators as well as pistons must be performed. This section provides the description and the models of these components.

Valve Model

Positive displacement pump valves are designed to be self-acting components. The motion of the valve is dependent on the upstream and downstream pressures, the fluid motion itself, the spring, and the preload force. The motion of the valve is important because it will control the flow area through which the fluid is forced and therefore the velocity. To calculate the valve gap velocity the energy equation (7) is used, where: p_{up} is the pressure upstream, p_{down} is the pressure downstream, ρ the fluid density, u the velocity of the fluid that crosses the valve, ζ_i the losses of the valve, empirical data calculated from Thield [40] and Johnston [5], [6], and l_{gap} is the length of the gap formed when the valve is open.

$$(p_{up} - p_{down}) + \frac{\rho u^2}{2}(1 + \sum\zeta_i) + \rho\frac{\partial u}{\partial t}l_{gap} = 0 \qquad (7)$$

This equation (6) considers the control volume of the valve itself and the solution is performed with an implicit Newton-Raphson method is used. The position of the valve (x_v), velocity and acceleration are calculated explicitly from the previous time step solving Newton's second law by the Adam-Bashforth leapfrog technique[41]. The forces considered to evaluate the valve motion are given in equation (8):

$$F_p + F_m + F_{pre} + F_D + F_s = m\ddot{x_v} \qquad (8)$$

Where the pressure force, F_p is calculated as $F_p = \psi A_V(p_{up} - p_{down})$ where A_V is the area of the valve where the pressure is acting, and ψ is the pressure force coefficient calculated from Johnston's work and Thiel [5], [6], [40]. The spring force, F_s, is related to the explicit position of the valve multiplied by the spring stiffness. F_m is the gravity force, the spring preload force, F_{pre}, meanwhile F_D is the damping force due to the fluid surrounding the valve itself. To calculate the flow rate across the valve, the area of the gap is computed geometrically from the valve characteristic (seat angle) and the valve position.

Accumulator Model

The accumulator is a hydraulic component used to smooth pressure fluctuations by absorbing the fluid energy in a compressible gas or spring and returning it when needed. It is a self-adjusting system, and it normally consists of two compartments created by a bladder, piston, disc, or diaphragm that separate the hydraulic fluid from the retained energy mechanism. Considering for instance the bladder gas accumulator, the accurate modelling of this apparatus should consider the compressibility of the gas and the rigidity of the diaphragm. The compressibility of the gas can be modelled as an ideal gas as a first approximation, although differences due to high pressure could occur [42]. This approach produces inaccuracy when the volume of the gas is at its minimum or maximum. When the accumulator pressure reaches the maximum, no more mass inflow can occur, and the gas or the spring cannot further compress. To prevent discontinuities, this consideration must be translated into a continuous function that diminishes the amount of fluid permitted inside the volume as the fluid reaches the maximum volume allowed by the compressibility of the system. If not properly modelled an artificial spurious interruption of the fluid could create unphysical waves in the system and mislead the results. Similar behaviour must be considered when the maximum volume of the gas or the elongation of the spring is reached. In this condition, no fluid is stored in the hydraulic system and a zero-mass flow rate boundary must be included. Therefore, an accurate model of the accumulator is complex and requires significant computational effort to be simulated correctly. In addition, to simplify the accumulator model a range of pressures where the ideal gas formulation (9) can be considered valid overall is assumed. Corrections functions are implemented when these limits are overtaken.

$$p_{gas}\left(V_{tot}-V_{fluid}\right)^{K}=p_{g_0}V_{tot}^{k} \qquad (9)$$

The accumulator is connected to the suction and discharge pipe with a tee junction where the information on the mass flow rate and the pressure is calculated. The shared information across the pipe is developed according to the continuity formulation and the wave travel information.

Pump Piston Model

The pump piston is modelled as a velocity boundary condition and the volume displaced from the piston motion is neglected. This assumes column fluid theory and simplifies the system, allowing the velocity of the fluid to be the same as the piston, $\dot{x_p}$. This simplification is valid until the fluid wave speed is significantly higher than the piston speed and will require the pressure wave dynamics to be accounted for. This piston speed is well below the fluid wave speed hence the pumped mass flow rate is calculated using the piston velocity given by equation (1) times the piston area and the fluid density calculated at the piston.

Stability Condition

To guarantee the convergence of the solution, the numerical stability must be checked. For an explicit scheme, a necessary but not sufficient condition is the Courant inequality, CFL [31], where the relation between the speed of sound, the time and the space grid must be less or equal to one: $\frac{c\,\Delta t}{\Delta x} \leq 1$. This inequality guarantees that the information wave travels inside the time-space grid and does not distort the information. In addition, a stability check must be provided for all solution methods used to solve the system. In detail, the integration scheme Adam-Bashforth (AB) used for the motion of the valves, the Runge Kutta fourth-order (RK4) method for the ODE and the MUSCL scheme algorithm for the PDE. The Adam-Bashforth is a linear multistep method meanwhile the Runge-Kutta method is a multi-stage method. Both methods can be rewritten as a function of the previous time steps.

$$U^n = \sum_i^k \theta_i U^{n-1} + \Delta t \sum_i^k \left(\Omega_i f\left(U^{n-i}\right)\right) \quad (10)$$

The multi-stages increase stability with the order of accuracy, differently, the linear multistep methods decrease stability by increasing the order of accuracy [41] therefore the stability condition could be performed only for AB, since the RK4 will be stable accordingly. The stability condition of these methods is determined by the solution of its characteristic polynomial $|P(U)| \leq 1$ that is always verified since the explicit MUSCL scheme requires a smaller time step than for the other algorithms. Therefore, the CFL condition is more restrictive than the other stability condition.

Test Setup

Model validation was performed with two different test rig configurations: a single-diaphragm pump actuated by a hydraulic piston and a three-chamber diaphragm pump each actuated hydraulically by a mechanical piston like the configuration in Figure (1).

A single diaphragm pump is the simplest configuration available where no suction and discharge chamber interaction occurs.

Figure 5 – Test rig for single chamber pump, where in red circle are highlight two piezo resistance sensors (at the suction and the discharge valves) and in green the piezoelectric sensor for the chamber pressure value.

The test rig for the single pump network can be seen in Figure 5. The system consists of a closed loop where the discharge pressure can be increased by the closure of different valves and orifices in a choke station. A schematic view of the pump loop is reported in Figure 6.

Three pressure sensors were used to collect data: two Sensortec A-105 piezo resistance sensors, one mounted before the suction valve and the other after the discharge valve (red circle in Figure 5), while the third was a Kistler 6005 piezoelectric sensor with a 5011B amplifier positioned in the chamber (green circle in Figure 5). In addition, the position of the piston and the diaphragm were measured by an Omega linear position sensors embedded in the piston connecting rod.

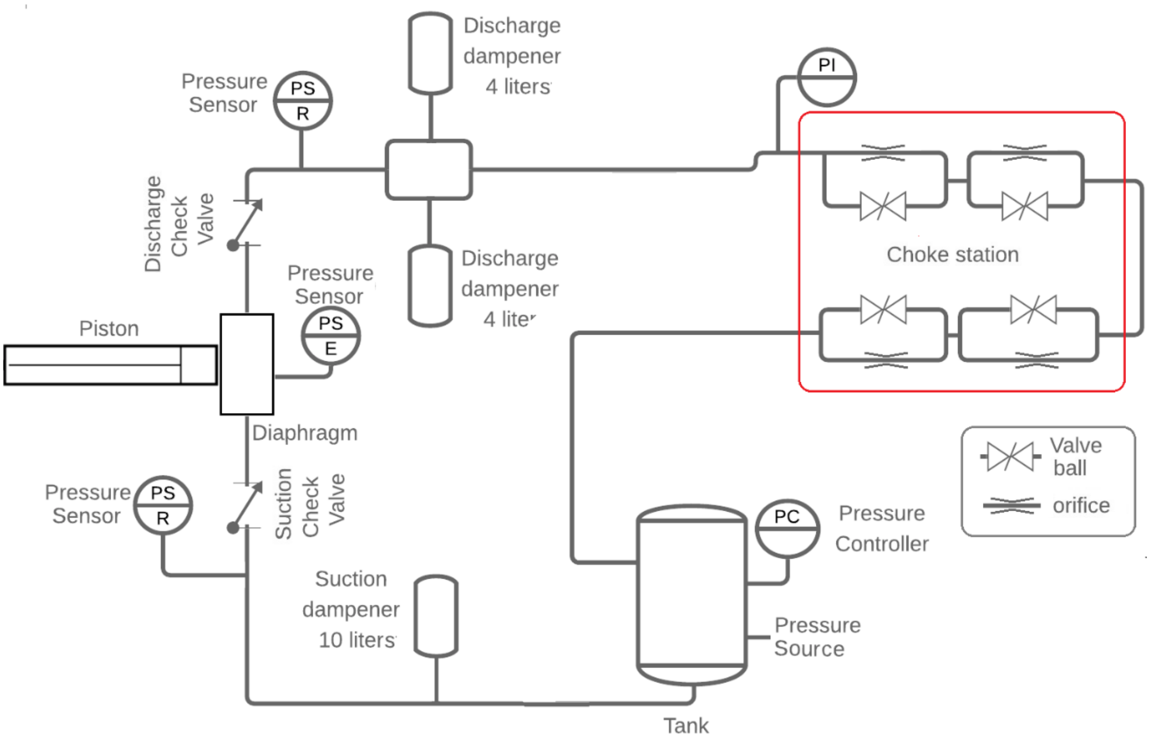

Figure 6 – Single chamber pump pressure loop

The system was controlled, and data were collected by the Supervision Control Data Acquisition (SCADA) system. The acquisition was performed at 9600 Hz (three times faster than the highest system frequency) to ensure the capture of wave reflection and possible cavity collapse. The fluid pumped was clean water (with an estimated speed of sound of 1250 m/s) meanwhile the propelling fluid was mineral oil (with an estimated speed of sound of 1300m/s). Four suction pressure conditions, from 1 to 4 bar, and three different piston speeds, strokes per minute (SPM), were investigated for a total of 12 sets of test data.

Increasing the SPM increases the velocity of the fluid especially across the suction valve (reducing the static pressure) increasing the eventuality of cavitation formation. With the same idea, we change the suction gauge pressure at the tank, relative to the vapour pressure to increase the cavitation behaviour. Although pumps are not likely to work in a condition where high SPM and low suction pressure are performed, this condition was performed as a challenge validation. For clarify, the compression phase occurs between 0 and 180 degrees and the suction phase from 180 to 0 degrees.

Due to the difficulties in experimentally evaluating the magnitude of the vapour phase, especially in the three-chamber configuration, the calculation and the performance of the cavity formations are inferred indirectly by pressure measurement. The pressure at the upstream side of the suction valve must drop lower than the downstream to lift the valve itself and suck the fluid in the chamber. The pressure at this stage can reach the vapour pressure stays almost constant at this value until a recovery pressure phase is reached. This condition occurs during the initial phase of the suction. The collapse of the cavity will produce a rapid decrease in bubble size resulting in an intense localized pressure increase [38], [43], [44]. Therefore, the cavitation period which occurs during the suction phase can be discerned experimentally between the minimum pressure reached and the highest peak reached immediately after. The series of pressure spikes after the first one can be considered unrelated to cavitation formation.

The one-chamber pump was tested in a controlled closed-loop test rig, where load pressure and suction pressure were easily controlled. Differently, the three-chamber diaphragm pump data acquisition was performed in an industrial application where the pump was part of a bigger network. Here, the SPM could be adjusted, differently the suction and the discharge pressure were dictated by the all-network system. The three-chamber pump configuration is shown in Figure 7. In addition, in this context, due to commercial confidentiality, the maximum pressure and mass flow rate cannot be given and thus the data have been provided normalised with maximum pressure and pump speed.

All experiments were repeated 60 times to have a wide range of repeatability and average data, in addition, data are presented with a red band within which the experiment is 95 per cent consistent, and a red solid line for the average value. For the sensors their sensitivity is 10 pC/bar.

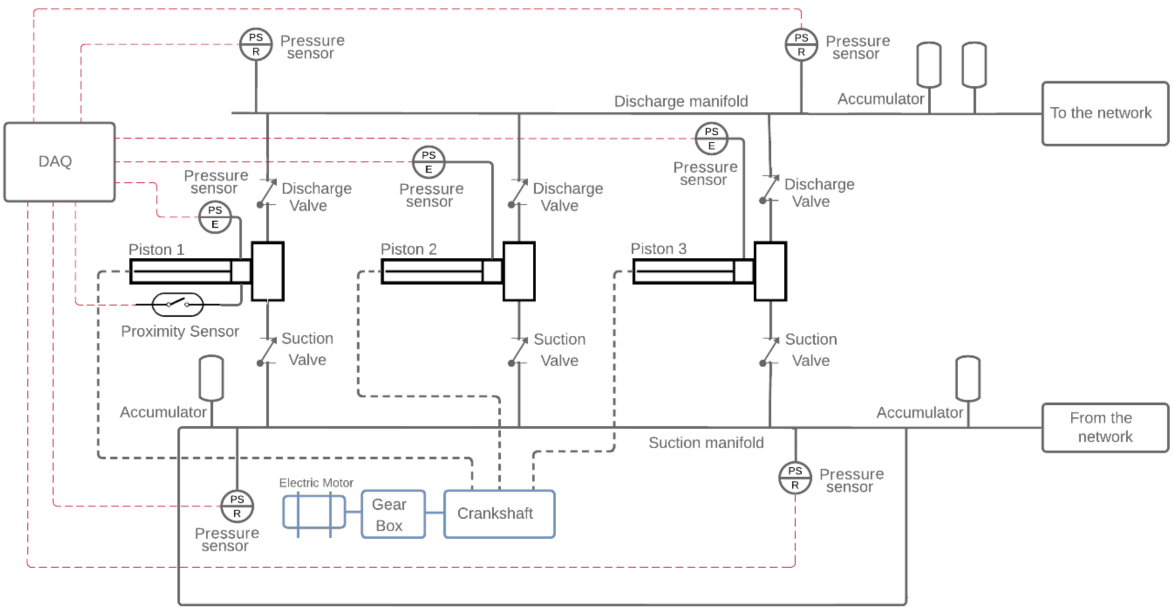

Figure 7 – Three chamber pump system schematic.

Results and discussion

The simulations, encompassing both single and three-chamber pumps, were executed on hardware equipped with an i7-6560U CPU @ 2.20 GHz and 16 GB of RAM. To ensure the numerical stability of ordinary differential equation integration, the Courant number was set to 0.9 in accordance with[37]. The initial condition for the non-dissolved gas was established with a volume fraction, denoted as α_g, set to 1e-7. The speed of sound in water was calculated based on the bulk modulus and allowed to vary with pressure, while for oil, a constant velocity of 1500 m/s was assumed. These computational settings and initial conditions were chosen to facilitate accurate and stable simulations of the pump system dynamics. Experimental and numerical simulations are correlated with the linear Pearson correlation factor reported in equation 11.

$$r_{xy} = \frac{\sum_i^n p_{Exp_i} p_{Num_i} - n\overline{p_{Exp_i}} \cdot \overline{p_{Num_i}}}{\sqrt{\sum_i^n p_{Exp_i}^2 - n \cdot \overline{p_{Exp_i}}^2}\sqrt{\sum_i^n p_{Num_i}^2 - n \cdot \overline{p_{Num_i}}^2} \quad (11)$$

One chamber pump

The one-chamber pump was simulated for all different conditions, to evaluate the possible scenarios, from absent to high cavitation conditions.

Due to the small size of the piston and diaphragm chambers, the time grid size to simulate the pumps and satisfy the stability condition is in the order of 10^{-6} sec. That translates into a significant computational effort for long components. To mitigate the time requirements, the long discharge line was truncated before the choke station, and the water reservoir was not included. In other words, the load due to the orifice and the pipes are not simulated. The simulated pressure used as a boundary condition is directly set from the pressure sensor positioned before the choke station. Regarding the water tank, the entire reservoir was neglected, and the suction pressure value was set at the entrance of the accumulator. This simplification affects the reflection and attenuation of the waves due to the short length of the pipe and the changing area across the pipe and tank. However, from a numerical point of view, this approach should not drastically change the system behaviour since the pressure at the reservoir remains almost constant. As reported in Iannetti et al. [2], [3] neglecting the tank and the entire suction line, the results are still in good agreement with the experimental data even for multi chambers pump.

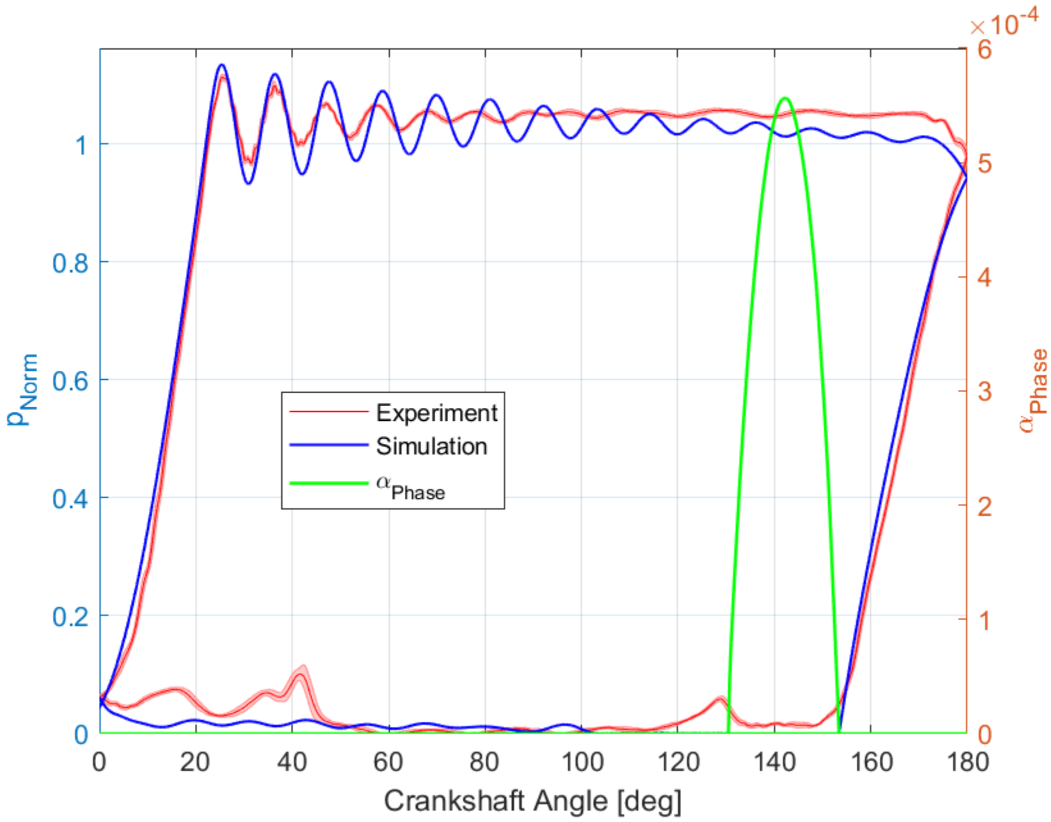

Figure 8 - Chamber pressure cycle of one chamber pump for SPM 75% and 2 bar of pressure, where the red line is the experimental data, the blue line is the simulation, and the green line is the second phase volume fraction overall produced.

Figure 8 shows the experimental and simulation chamber pressure comparison in terms of crank angle. The simulation considers 75% of the maximum stroke speed and 2 bar of suction pressure. The experiment and the numerical pressure profile match Pearson's correlation factor of $R_{xy} = 0.998$. The numerical calculation of the vapour phase formation, (green line) in Figure 8 agrees with the observed peak-to-peak experimental pressure between 155 and 120 deg. The discharge phase behaves as a second-order underdamped system disconnected from the suction circuit thanks to the choke station valves. The repeatability of the experiment shows a narrow band of error. Both experimental and numerical data show a pressure profile that stays constant at low pressure for the entire suction phase. Differences start to appear around 40 degrees where higher pressure fluctuations are present in the experiment. The authors believe that the effect is a potential drawback due to the lack of tank dynamic simulation. This peak pressure value is not interpreted as a cavitation phenomenon, since the velocity and the working suction pressure are in the specification of the pump performance. In the discharge phase, the pressure and the pulsation agree with the experiment. However, the pulsation dissipation is not as high as the experimental. This difference could be caused by the lack of a series of orifices used to create the pressure load, neglected in the simulation (red square in Figure 6). In addition, a further limitation could be given by the lack of a complex friction dissipation model, since the fluid model uses the simplified Darcy–Weisbach equation further investigation will be performed.

The frequency analysis for the same experiment agrees with the experiment as shown in Figure 9 where the red circle represents the experimental chamber intensity pressure value and the blue line the experimental. The algorithm predicts the harmonics correctly in terms of frequency and intensity, therefore even from the spectral analysis of view this algorithm proves its potential.

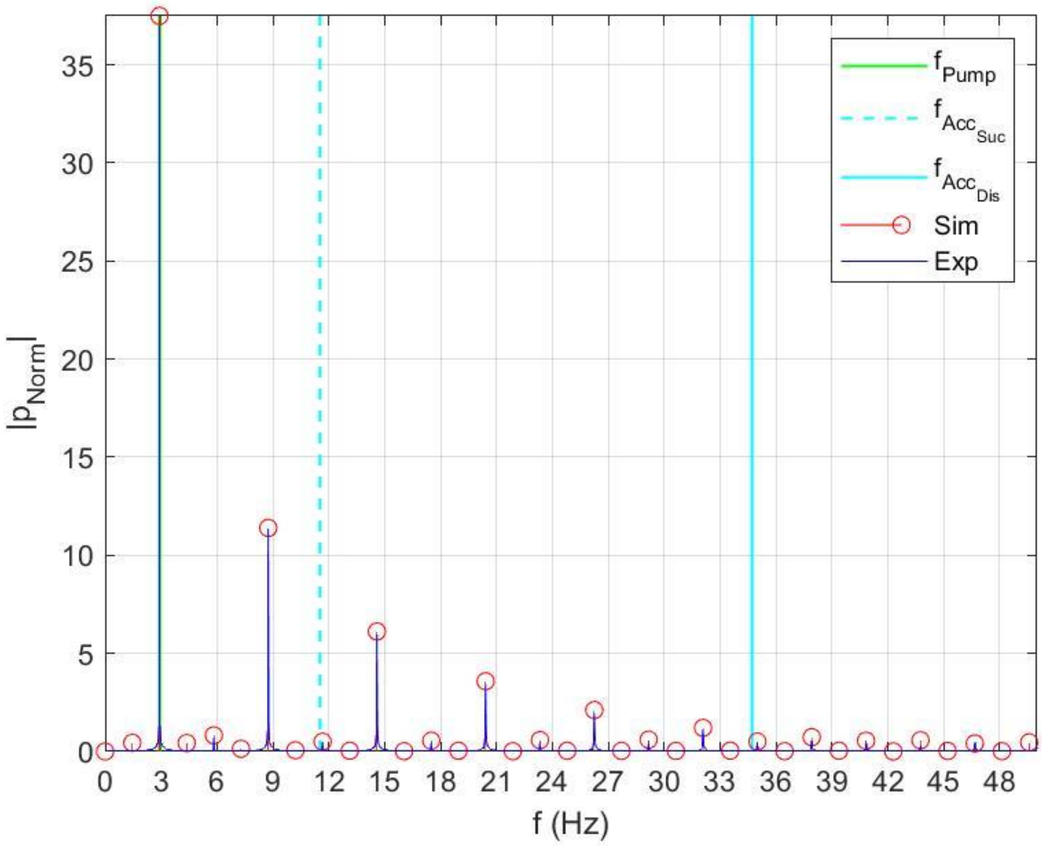

Figure 9 - Frequency pressure analysis for SPM 75% and pressure 0.25 of the maximum for of one chamber pump. The blue line is the numerical response, and the red dots are the experimental, meanwhile, the two light blue lines refer to the accumulators and the green to the pump frequency.

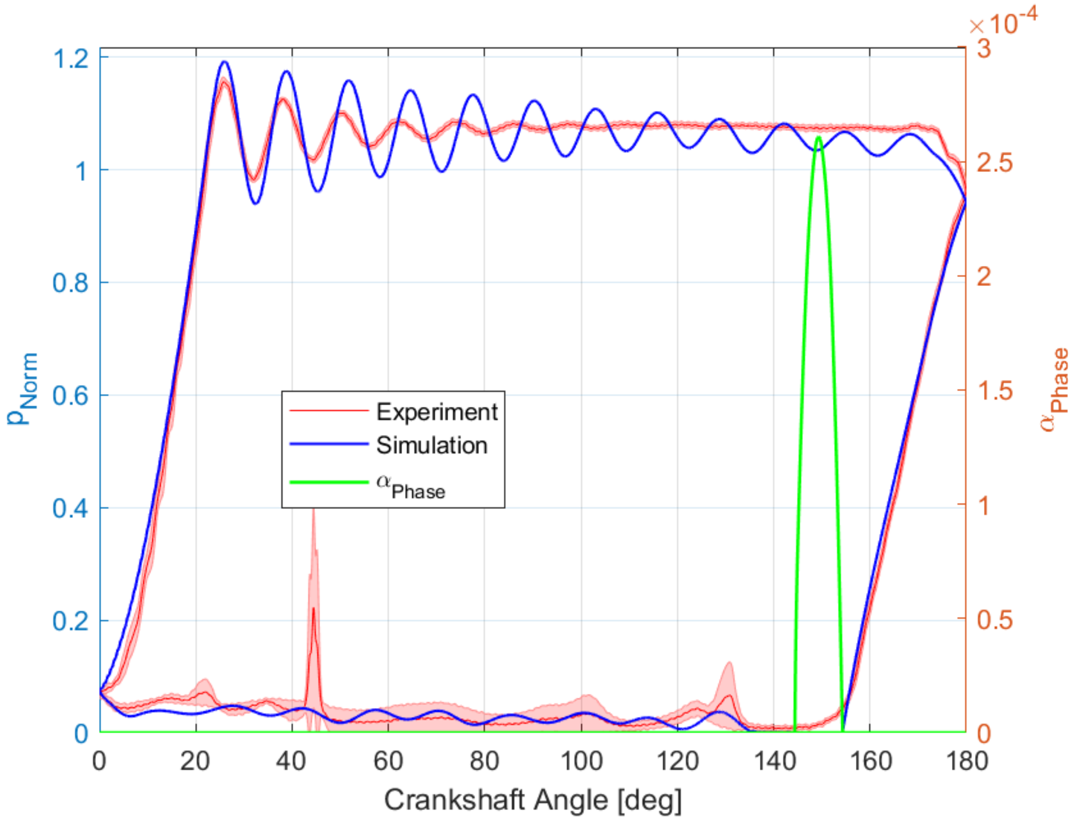

Figure 10 - Chamber pressure cycle of one chamber pump cycle for SPM 87.5% and 2 bar of pressure, where the red line is the experimental data, the blue line is the simulation and the green line is the second phase volume fraction overall produced.

Increasing the stroke speed of the pump to 87.5% of the max, the pressure response compares favourably as shown in Figure 10. The pressure pulsation at discharge is overestimated, highlighting once more the lack of dissipation phenomenon. The pressure in the suction pipe is similar, for most of the duration and the first peak at 125 degrees was depicted correctly, although the difference in the value is noted. The pressure profile, after the gas void collapsing follows the experimental trend. The pressure stays almost constant at the vapour pressure value until 120 degrees, a phenomenon reported also in Figure 8. The experimental data uncertainties show a wider band for the suction showing a more difficult repeatability in the high-speed pump.

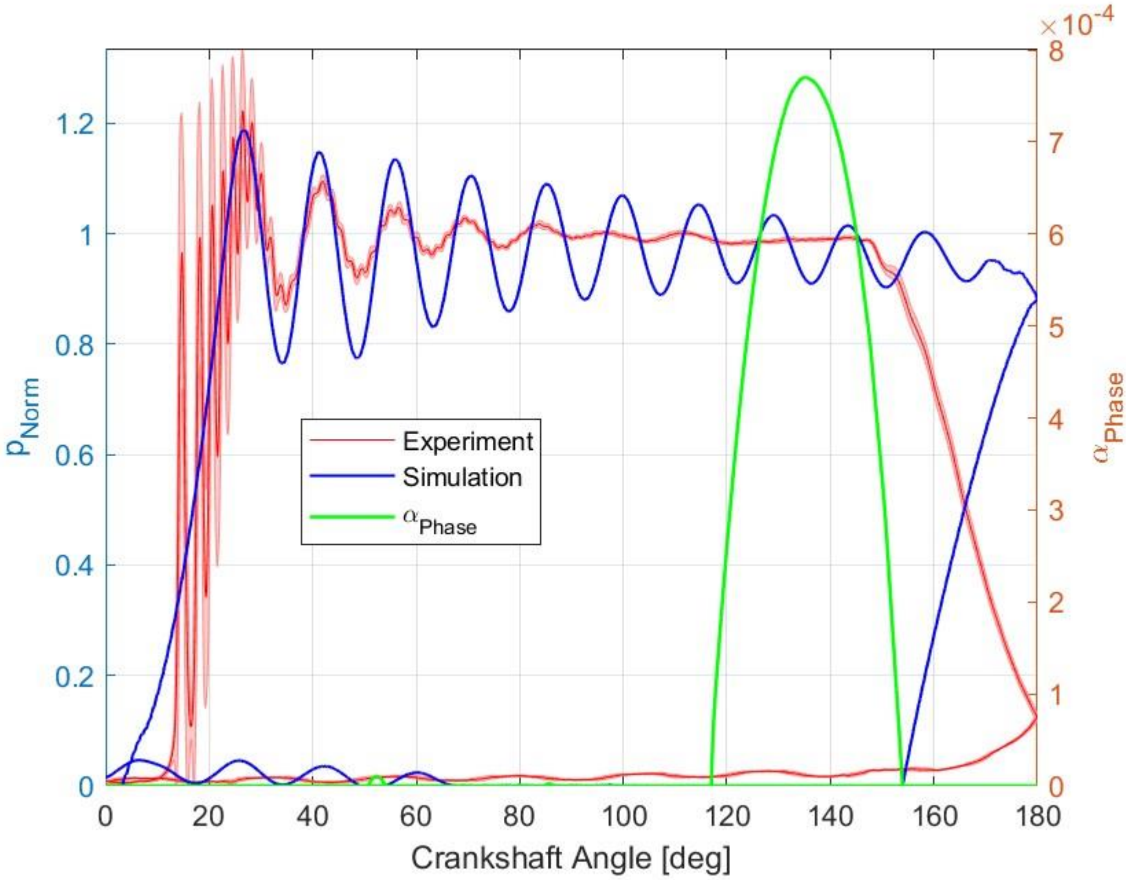

Figure 11 – Chamber pressure cycle of one chamber pump for SPM 100% and 1 bar of pressure, where the red line is the experimental data, the blue line is the simulation and the green line is the second phase volume fraction overall produced.

Significant differences occur when void formation affects the discharge phase. In Figure 11, the differences in the predicted and experimental pressures are shown. In the experimental data, the vapour is generated throughout all the suction phases where the pressure is constant well beyond the 180 degrees of the crankshaft. The cycling profile is strongly affected by the vapour-phase formation resulting in a series of collapses and high peak pressure. The experimental suction phase (red line) starts around 170 degrees, and the pressure is at the vapour pressure for the entire suction phase. When the discharge phase occurs and the piston changes direction (20 degrees) the collapse of the bubble occurs due to mechanical compression, resulting in pressure fluctuations and creating high peak pressure. These effects are not predicted by the algorithm, that underestimates the cavities produced limiting its cavitation performance range. Therefore, this methodology is unfeasible in extreme cavity conditions. However, it should be pointed out, that pumps should never run at this level because structural failure can occur.

An overall comparison of predicted and tests can be achieved by examining the pump efficiency. Using the Tackett formulation 10 [45], the value of the efficiency is calculated as 84%, since this formulation is not condition dependent. This formulation does not consider backflow formation, leakage and cavitation. The function considers only the maximum and the minimum pressure, the fluid bulk modulus, the ratio of total volume and displacement volume, and valve losses (estimated at 3%).

$$\eta_{vol_{Tack}} = 1 - (p_{Max} - p_{Min})\beta\rho + V_L \tag{6}$$

The simulated pump gives similar values, as reported in Table 2, albeit doubts about the validity of case 12 arise due to the high cavity formation. In detail, the simulation considers all possible backflow, compressibility and losses due to cavitation.

Table 2 - One chamber pump volumetric efficiency

#	Case	η_{vol}
1	$P_{suction} = 4\ bar,\ SPM = 100\%$	82.59
2	$P_{suction} = 3\ bar\ ,SPM = 100\%$	82.52
3	$P_{suction} = 2\ bar, SPM = 100\%$	82.18
4	$P_{suction} = 1\ bar, SPM = 100\%$	82.16
5	$P_{suction} = 4$ bar $SPM = 87.5\%$	82.27
6	$P_{suction} = 3$ bar $SPM = 87.5\%$	82.36
7	$P_{suction} = 2$ bar $SPM = 87.5\%$	82.08
8	$P_{suction} = 1$ bar $SPM = 87.5\%$	82.09
9	$P_{suction} = 4$ bar $SPM = 75\%$	82.09
10	$P_{suction} = 3$ bar $SPM = 75\%$	82.27
11	$P_{suction} = 2$ bar $SPM = 75\%$	82.33
12	$P_{suction} = 1$ bar $SPM = 75\%$	80.93

Three chamber pump

From a computational point of view, multiple chamber pumps are challenging. The need to initialise correctly each component of the chambers and their mutual interaction is the major issue. A one-chamber pump can be initialized as completely steady, for multiple-chamber pumps that is unfeasible. Considering a three-chamber pump with a 120-degree shift between the chambers implies a different starting condition. When one chamber is at the suction phase with all valves closed, the other chamber is either compressing or decompressing, and one of the valves could also be in the open position. From a numerical point of view, this implies knowing exactly the behaviour of the pump chambers in terms of fluid velocity, temperature, density, pressure in all the cells, valve velocity and position on each chamber, and the gas pressure of the accumulator. In case of moving mesh algorithms the initialization became extreme difficult. To address this issue, there are different possible solutions, however, most of them are impractical for full three-dimensional analysis. The one-dimensional analysis, on the contrary, can address this issue due to its simplicity and fast computational times. It is possible to simulate the run-up of the entire pump as in the real pump motion with reasonable computational efficiency. Figure 12 is an example of a run-up for a three-chamber pump, where the velocities of the three different pistons are depicted.

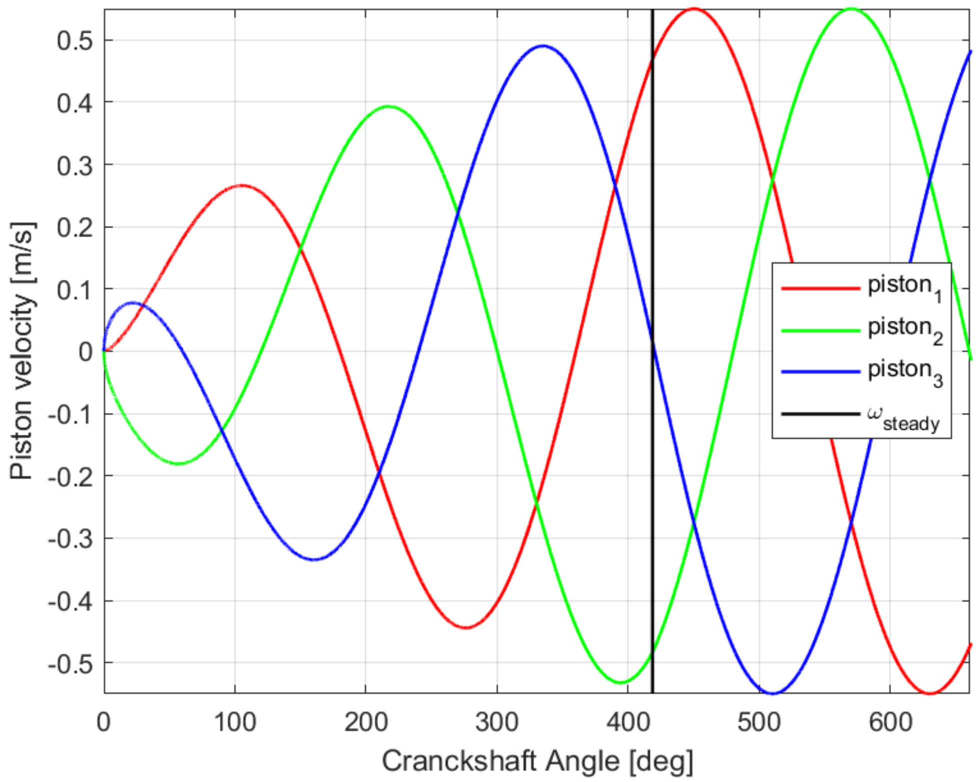

Figure 12 - Example of three-chamber pump piston velocity vs crankshaft angle, where red line is the reference piston at 0 degrees, the blue and the green are respectively at 120, and -120 degrees position. The black line indicates when the angular velocity reach the steady condition.

Differently from one chamber pump, in this context, the experimental data are affected by multiple factors due to the more complex system network. The pump analysed here is one of the multi-pump systems with variable boundary conditions set from the pipeline networks. These effects are seen in all the experimental results with noise and low-frequency responses, and the simulation can depict only part of them. In contrast to the single-chamber pump, a further complication on the valves is their opening and closing behaviour influenced by the out-of-phase suction and discharge on the other pumping chambers. This is due to the common suction and discharge plenum. Thus, in a multiple pumping chamber simulation, the fidelity of the simulations is more sensitive to the entire system dynamics.

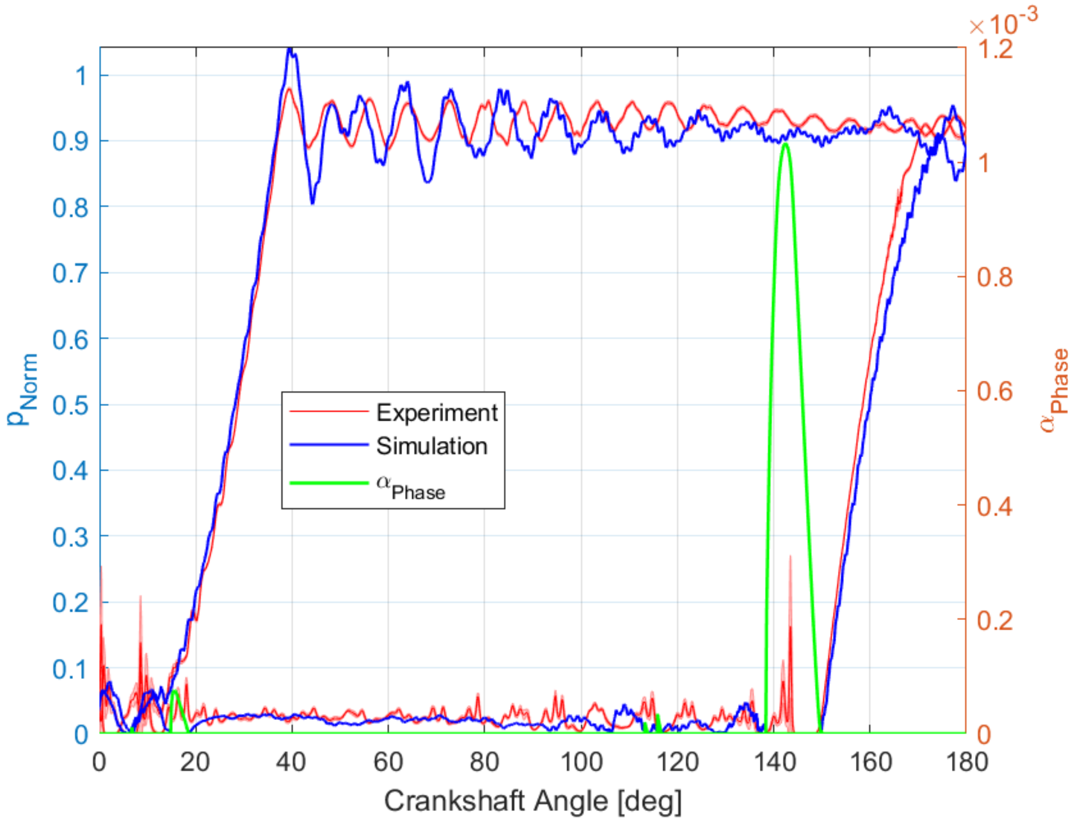

Figure 13 – Chamber pressure cycle of three chamber pump for SPM 100% and 4 bar of suction pressure, where the red line is the experimental data, the blue line is the simulation and the green line is the second phase volume fraction overall produced.

Figure 13 shows the pressure history for chamber 1 for a high-speed and low-pressure suction test. The simulated behaviour did not capture the pressure fluctuations in the discharge phase. On the contrary, mutual interaction in the discharge is predicted with high fidelity at 160 degrees in the discharge phase. Similar behaviour for the suction phase is simulated, although the interference with the other chambers and system is much higher for the experimental data than in the simulation. Cavity formation seems reasonably in agreement with the experimental pressure behaviour, although a slight phase shift is depicted. Considering the cavity formation, this system depicts a reasonable amount of vapour, which agrees with the experiment's peak-to-peak.

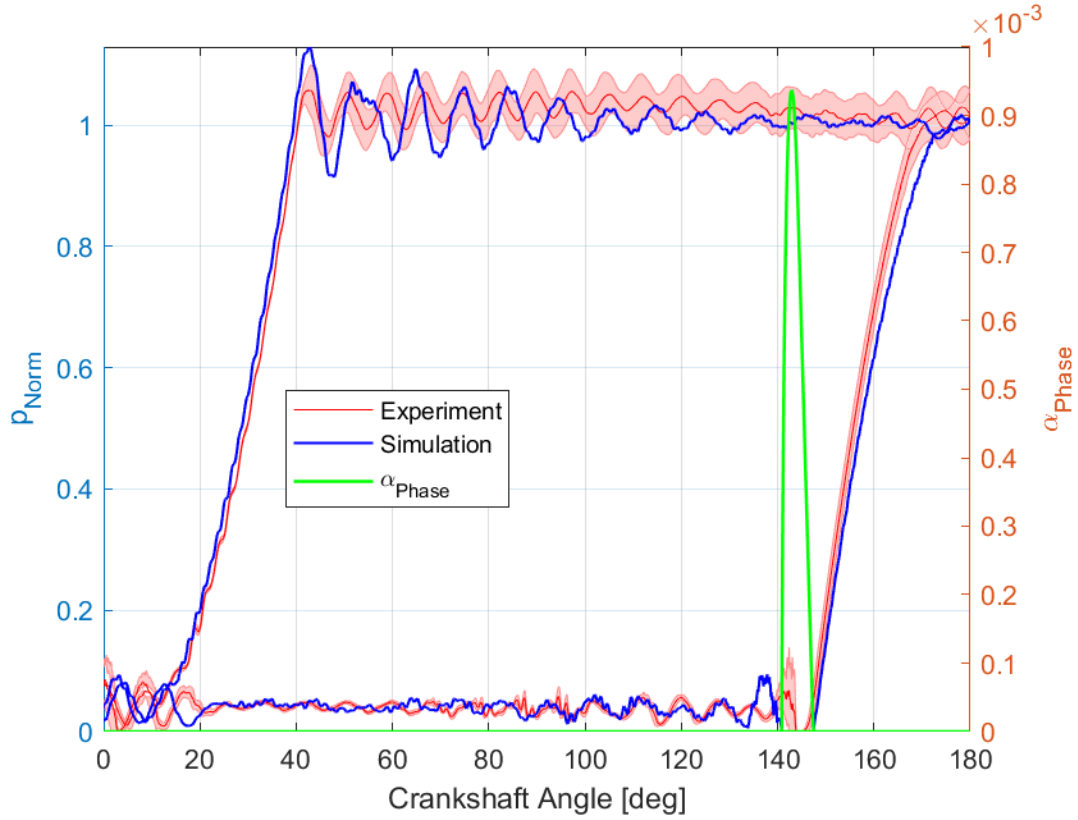

Figure 14 Chamber pressure cycle of three chamber pump for SPM 100% and 8 bar of suction pressure, where the red line is the experimental data, the blue line is the simulation and the green line is the second phase volume fraction overall produced.

Figure 14 shows the experimental result for a high suction pressure and the maximum speed of the pump. At the discharge phase, the experimental pressure is affected by a low-frequency response not shown in the simulation of the accumulators. The complexity of the network, as well as pressure fluctuation in the discharge line (and in the suction line), is difficult to predict and noise is evident.

Although the amount of cavitation produced cannot be identified experimentally, once more the cavitation period agrees with peak-to-peak pressure. In conclusion, Table 3 reports the Pearson correlation factor for all the experiments produced for the three-chamber pump. Despite the complexity of the system, a close correlation between the experimental data and the computational simulation (pre-normalization) has been achieved.

Table 3 – Pearson correlation factor for three-chamber pump

SPM [%}	***Max Suction pressure***	***Min Suction pressure***
100	0.962	0.967
60	0.956	0.962
40	0.962	0.958

The overall system has required the simulation of all components including valves and accumulators. During the suction valve opening phase, the pressure velocity must increase, and the static pressure is reduced accordingly. This dynamic response is strongly dependent on the valve characteristics [8], therefore the simplification inherent in a one-dimensional approach could reduce the overall simulation performance. However, in this context as well as the one-chamber pump, the entire algorithm provides enough accuracy to be used as cavitation and performance pump prediction even in complex network.

Conclusion

The study has highlighted the efficacy of a one-dimensional analysis in capturing crucial aspects of positive displacement (PD) pump fluid dynamics under both normal and cavitating conditions. The algorithm exhibited a high level of fidelity in replicating experimental results, instilling confidence in its potential for practical implementation within an industrial setting. Leveraging the finite volume method with a TVD scheme, the code's simplicity, and its adaptability for various applications suggest a broad scope for extension to different types of positive displacement pumps and diverse operational environments.

The results underscore that the dominant factor influencing pump phenomena is the piston motion, given the higher relative information speed compared to perturbations. However, this dynamic changes when the speed of sound becomes comparable to perturbations, particularly in scenarios with a high-volume fraction of the second phase, as observed in high-cavitation environments for single pumps. Further investigation to assess this aspect should be performed.

While the compressible model was employed for all scenarios, the investigation revealed low compressibility of the pure fluid under the pressure conditions examined. This limitation implies that the algorithms were not tested across their full capability range. Further research, particularly in the context of hydraulic fracking pumps where fluid compressibility is more pronounced, is warranted.

Additionally, the algorithm's evaluation of pressure pulsations in the frequency domain showcased its potential to assess harmonic responses, even in the presence of a second phase. A comparison with a three-dimensional model demonstrated that while this method offers reasonable accuracy at a faster pace, it sacrifices some local phenomena details, especially in complex systems involving valves and accumulators with intricate three-dimensional interactions.

Future enhancements should focus on incorporating different vapour and cavity algorithms to broaden the code's capabilities, especially in scenarios with high cavity performance. Furthermore, addressing the limitations observed in friction dissipation under quasi-steady conditions necessitates ongoing research to refine loss predictions.

In summary, the algorithm aligns reasonably well with experimental results, establishing itself as a valuable design and diagnostic tool for extensive use in industrial environments. Its versatility allows for the straightforward implementation of optimization algorithms and prognostic simulations, marking it as a promising asset for advancing pump system analysis and performance optimization.

References

[1] R. van Rijswick, “Fluid structure interaction in piston diaphragm pumps,” Delft University of Technology, 2017. doi: 10.4233/uuid:2f24e261-003f-4e80-ba4e-0b0c1caecdf7.

[2] A. Iannetti, M. T. Stickland, and W. M. Dempster, “A CFD and experimental study on cavitation in positive displacement pumps: Benefits and drawbacks of the ‘full’ cavitation model,” *Engineering Applications of Computational Fluid Mechanics*, vol. 10, no. 1, pp. 57–71, Jan. 2016, doi: 10.1080/19942060.2015.1110535.

[3] A. Iannetti, M. T. Stickland, and W. M. Dempster, “A computational fluid dynamics model to evaluate the inlet stroke performance of a positive displacement reciprocating plunger pump,” *Proceedings of the Institution of Mechanical Engineers,*

Part A: Journal of Power and Energy, vol. 228, no. 5, pp. 574–584, Aug. 2014, doi: 10.1177/0957650914530295.

[4] K. M. Opitz, S. R. Engel, A. F. Koegler, A. Leipertz, and E. Schlücker, "High-Speed Particle Image Velocimetry Measurements of Turbulent Pipe Flows for Verification of a Fluid-Dynamic Cavitation Model," *Chem Eng Technol*, vol. 35, no. 11, pp. 2035–2044, Nov. 2012, doi: 10.1002/ceat.201200209.

[5] D. N. Johnston, "Numerical Modelling of Reciprocating Pumps with Self-Acting Valves," *Proceedings of the Institution of Mechanical Engineers, Part I: Journal of Systems and Control Engineering*, vol. 205, no. 2, pp. 87–96, May 1991, doi: 10.1243/PIME_PROC_1991_205_318_02.

[6] D. N. Johnston, K. A. Edge, and N. D. Vaughan, "Experimental Investigation of Flow and Force Characteristics of Hydraulic Poppet and Disc Valves," *Proceedings of the Institution of Mechanical Engineers, Part A: Journal of Power and Energy*, vol. 205, no. 3, pp. 161–171, Aug. 1991, doi: 10.1243/PIME_PROC_1991_205_025_02.

[7] X. Song, L. Cui, M. Cao, W. Cao, Y. Park, and W. M. Dempster, "A CFD analysis of the dynamics of a direct-operated safety relief valve mounted on a pressure vessel," *Energy Convers Manag*, vol. 81, pp. 407–419, May 2014, doi: 10.1016/j.enconman.2014.02.021.

[8] W. Li and Z. Yu, "Cavitating flows of organic fluid with thermodynamic effect in a diaphragm pump for organic Rankine cycle systems," *Energy*, vol. 237, p. 121495, Dec. 2021, doi: 10.1016/j.energy.2021.121495.

[9] W. Li and Z. Yu, "Cavitating flows of organic fluid with thermodynamic effect in a diaphragm pump for organic Rankine cycle systems," *Energy*, vol. 237, p. 121495, Dec. 2021, doi: 10.1016/j.energy.2021.121495.

[10] Y. W. Shin and W. L. Chen, "Numerical fluid-hammer analysis by the method of characteristics in complex piping networks," *Nuclear Engineering and Design*, vol. 33, no. 3, pp. 357–369, Sep. 1975, doi: 10.1016/0029-5493(75)90005-9.

[11] R. van Rijswick, A. Talmon, and C. van Rhee, “Fluid structure interaction (FSI) in piston diaphragm pumps,” *Can J Chem Eng*, vol. 94, no. 6, pp. 1116–1126, Jun. 2016, doi: 10.1002/cjce.22487.

[12] A. Josifovic, M. Stickland, A. Iannetti, and J. Corney, “Engineering Procedure for Positive Displacement Pump Performance Analysis Based on 1D and 3D CFD Commercial Codes,” in *Volume 1: 37th Computers and Information in Engineering Conference*, American Society of Mechanical Engineers, Aug. 2017. doi: 10.1115/DETC2017-67758.

[13] S. M. Price, D. R. Smith, and J. D. Tison, “The Effects Of Valve Dynamics On Reciprocating Pump Reliability,” *Turbomachinery and Pump Symposia*, 1995, doi: 10.21423/R1T98V.

[14] J.-J. Shu, C. R. Burrows, and K. A. Edge, “Pressure pulsations in reciprocating pump piping systems Part 1: Modelling,” *Proceedings of the Institution of Mechanical Engineers, Part I: Journal of Systems and Control Engineering*, vol. 211, no. 3, pp. 229–235, May 1997, doi: 10.1243/0959651971539768.

[15] J. K. Lee, J. K. Jung, J.-B. Chai, and J. W. Lee, “Mathematical modeling of reciprocating pump,” *Journal of Mechanical Science and Technology*, vol. 29, no. 8, pp. 3141–3151, Aug. 2015, doi: 10.1007/s12206-015-0713-x.

[16] K. A. Edge, O. P. Boston, K. C. S. Xiao, K. C. M. J. Longvill, and K. C. C. R. Burrows, “Pressure pulsations in reciprocating pump piping systems Part 2: Experimental investigations and model validation,” *Proceedings of the Institution of Mechanical Engineers, Part I: Journal of Systems and Control Engineering*, vol. 211, no. 3, pp. 239–250, May 1997, doi: 10.1243/0959651971539777.

[17] P. J. Singh and N. K. Madavan, “Complete Analysis And Simulation Of Reciprocating Pumps Including System Piping,” 1987. [Online]. Available: https://api.semanticscholar.org/CorpusID:117452406

[18] G. Vetter and F. Schweinfurther, “Pressure pulsations in the piping of reciprocating pumps,” *Chem Eng Technol*, vol. 10, no. 1, pp. 262–271, Jan. 1987, doi: 10.1002/ceat.270100132.

[19] A. R. Lohrasbi and R. Attarnejad, "Water Hammer Analysis by Characteristic Method," *American Journal of Engineering and Applied Sciences*, vol. 1, no. 4, pp. 287–294, Apr. 2008, doi: 10.3844/ajeassp.2008.287.294.

[20] K. S. Sumam, S. G. Thampi, and N. Sajikumar, "An alternate approach for modelling of transient vaporous cavitation," *Int J Numer Methods Fluids*, vol. 63, no. 5, pp. 564–583, Jun. 2010, doi: 10.1002/fld.2093.

[21] M. H. Chaudhry and M. Y. Hussaini, "Second-Order Accurate Explicit Finite-Difference Schemes for Waterhammer Analysis," *Journal of Fluids Engineering-transactions of The Asme*, vol. 107, pp. 523–529, 1985, [Online]. Available: https://api.semanticscholar.org/CorpusID:120164246

[22] A. Bergant, A. S. Tijsseling, J. P. Vítkovský, D. I. C. Covas, A. R. Simpson, and M. F. Lambert, "Parameters affecting water-hammer wave attenuation, shape and timing—Part 1: Mathematical tools," *Journal of Hydraulic Research*, vol. 46, no. 3, pp. 373–381, May 2008, doi: 10.3826/jhr.2008.2848.

[23] A. Bergant, A. Ross Simpson, and J. Vìtkovsk[ygrave], "Developments in unsteady pipe flow friction modelling," *Journal of Hydraulic Research*, vol. 39, no. 3, pp. 249–257, Jul. 2001, doi: 10.1080/00221680109499828.

[24] B. Milanjit, D. S. Mimi, and M. Das Madan, "Development of Numerical Model for Transients in pipe flow for Water Hammer situation and comparison of different friction equations for transient friction," *International Research Journal of Engineering and Technology*, Mar. 2018.

[25] M. Zhao and M. S. Ghidaoui, "Godunov-Type Solutions for Water Hammer Flows," *Journal of Hydraulic Engineering*, vol. 130, no. 4, pp. 341–348, Apr. 2004, doi: 10.1061/(ASCE)0733-9429(2004)130:4(341).

[26] A. S. León, M. S. Ghidaoui, A. R. Schmidt, and M. H. García, "Efficient Second-Order Accurate Shock-Capturing Scheme for Modeling One- and Two-Phase Water Hammer Flows," *Journal of Hydraulic Engineering*, vol. 134, no. 7, pp. 970–983, Jul. 2008, doi: 10.1061/(ASCE)0733-9429(2008)134:7(970).

[27] S. SaemI, M. Raisee, M. J. Cervantes, and A. Nourbakhsh, “Computation of two- and three-dimensional water hammer flows,” *Journal of Hydraulic Research*, vol. 57, no. 3, pp. 386–404, May 2019, doi: 10.1080/00221686.2018.1459892.

[28] Y. Hwang and N. Chung, “A fast Godunov method for the water-hammer problem,” *Int J Numer Methods Fluids*, vol. 40, no. 6, pp. 799–819, Oct. 2002, doi: 10.1002/fld.372.

[29] L. Zhou, H. Wang, D. Liu, J. Ma, P. Wang, and L. Xia, “A second-order Finite Volume Method for pipe flow with water column separation,” *Journal of Hydro-environment Research*, vol. 17, pp. 47–55, Dec. 2017, doi: 10.1016/j.jher.2016.11.004.

[30] L. Zhou, Y. Li, B. Karney, Y. Cheng, and D. Liu, “Godunov-Type Solutions for Transient Pipe Flow Implicitly Incorporating Brunone Unsteady Friction,” *Journal of Hydraulic Engineering*, vol. 147, no. 7, Jul. 2021, doi: 10.1061/(ASCE)HY.1943-7900.0001895.

[31] Malalasekera W. and H. K. Versteeg, *An introduction to computational fluid dynamics : the finite volume method*, 2nd ed. Pearson Education Ltd, 2007.

[32] M. S. Ghidaoui, M. Zhao, D. A. McInnis, and D. H. Axworthy, “A Review of Water Hammer Theory and Practice,” *Appl Mech Rev*, vol. 58, no. 1, pp. 49–76, Jan. 2005, doi: 10.1115/1.1828050.

[33] R. van Rijswick, “Fluid structure interaction in piston diaphragm pumps.” 2017. doi: 10.4233/uuid:2f24e261-003f-4e80-ba4e-0b0c1caecdf7.

[34] R. J. LeVeque, *Finite Volume Methods for Hyperbolic Problems*. Cambridge University Press, 2002. doi: 10.1017/CBO9780511791253.

[35] E. Goncalvès and B. Charrière, “Modelling for isothermal cavitation with a four-equation model,” *International Journal of Multiphase Flow*, vol. 59, pp. 54–72, Feb. 2014, doi: 10.1016/j.ijmultiphaseflow.2013.10.015.

[36] Vincent Guinot, *Wave Propagation in Fluids: Models and Numerical Techniques*. Wiley-ISTE, 2008.

[37] F. Rizzuto, M. Stickland, W. Dempster, and R. Van Rijswick, “One-Dimensional Compressible Solution for Transient Cavitating Pipe Flow,” *Journal of Hydraulic Engineering*, vol. 147, no. 4, Apr. 2021, doi: 10.1061/(ASCE)HY.1943-7900.0001855.

[38] C. E. Brennen, *Fundamentals of Multiphase Flow*. Cambridge University Press, 2005. doi: 10.1017/CBO9780511807169.

[39] A. Bergant, A. R. Simpson, and A. S. Tijsseling, “Water hammer with column separation: A historical review,” *J Fluids Struct*, vol. 22, no. 2, pp. 135–171, Feb. 2006, doi: 10.1016/j.jfluidstructs.2005.08.008.

[40] E. Thiel, *Kinematik und Druckverlust selbsttätiger Ventile oszillierender Verdrängerpumpen*. 1990. [Online]. Available: https://books.google.co.nz/books?id=sze1HAAACAAJ

[41] J. C. Butcher, *Numerical Methods for Ordinary Differential Equations*. Wiley, 2016. doi: 10.1002/9781119121534.

[42] S. Zhang, H. Iwashita, and K. Sanada, “Thermal performance difference of ideal gas model and van der Waals gas model in gas-loaded accumulator,” *International Journal of Hydromechatronics*, vol. 1, no. 3, p. 293, 2018, doi: 10.1504/IJHM.2018.094884.

[43] J. Luo and Z. Niu, “Jet and Shock Wave from Collapse of Two Cavitation Bubbles,” *Sci Rep*, vol. 9, no. 1, p. 1352, Feb. 2019, doi: 10.1038/s41598-018-37868-x.

[44] K. ANDO *et al.*, “Shock propagation through a bubbly liquid in a deformable tube,” *J Fluid Mech*, vol. 671, pp. 339–363, Mar. 2011, doi: 10.1017/S0022112010005707.

[45] H. H. Tackett, J. A. Cripe, and G. Dyson, “Positive Displacement Reciprocating Pump Fundamentals - Power And Direct Acting Types,” *Turbomachinery and Pump Symposia*, 2008.